Journal of Magnetic Resonance **157,** 69–73 (2002)
doi:10.1006/jmre.2002.2568

Combined k-Space q-Space Pulsed ESR Imaging: Mapping of Restricted Diffusion in $(FA)_2PF_6$

A. Feintuch,* T. Tashma,* A. Grayevsky,* J. Gmeiner,‡ E. Dormann,† and N. Kaplan*

*Racah Institute, Hebrew University, Jerusalem, Israel; †Physikalisches Institut, Universität Karlsruhe, (TH) D-76128 Karlsruhe, Germany; and ‡Physikalisches Institut and Bayreuther Institut für Makromolekülforschung (BIMF), Universität Bayreuth, Postfach 101251, D-95440 Bayreuth, Germany

E-mail: akivaf@vms.huji.ac.il

Received January 29, 2002; revised May 14, 2002

A $(FA)_2PF_6$ crystal from the family of the quasi-one-dimensional organic conductors was selectively damaged by a beam of Helium ions with a slitted mask placed in the beam's trajectory. Pulsed ESR density weighted imaging of the damaged crystal revealed the appearance of regions where the ESR signal was absent. The one-dimensional motion of the charge carriers was thus restricted to the undamaged sections. The local charge carrier spin dynamics in these restricted areas was probed by combined k-space q-space pulsed ESR imaging. The local expected appearance of the restricted pulsed gradient spin echo (PGSE) "diffusive diffraction" effect is shown. The position of the diffraction minima is compatible with the density imaging results.

Key Words: **k-space; q-space; PGSE; pulsed ESR; one-dimensional organic conductors.**

1. INTRODUCTION

The combination of spatial encoding magnetic field gradients and the pulsed gradient spin echo (PGSE) method is the standard procedure for probing local spin dynamics in nuclear magnetic resonance imaging (*1*). In this paper we apply this procedure using pulsed ESR imaging to study the motion of the charge carriers spin in the quasi-one-dimensional organic conductor $(FA)_2PF_6$ (FA, fluoranthene) (*2*).

ESR imaging has been attracting renewed attention due to the possibility of *in vivo* implementation. A detailed description of the latest developments has been presented in a recent review article by G.R. Eaton and S.S. Eaton (*3*). The imaging examples reported include a few cases of time domain pulsed ESR imaging (*4, 5*). These are usually based on the back projection reconstruction method which requires application of static gradients during signal detection. Recently we have reported on an implementation which incorporates phase encoding gradients applied prior to signal detection. The imaging is performed on the $(FA)_2PF_6$ crystals. The anisotropy of the electron spin mobility in these crystals requires a Cartesian encoding which is not possible with the back projection technique (*6*).

The PGSE sequence provides a mean for encoding spin translational motion. Integral PGSE measurements performed on the $(FA)_2PF_6$ crystals have shown that the spin motion along the conducting axis deviates from a free diffusion model and seems to be restricted, although attempts to fit the results to a restricted diffusion model have been successful only for part of the crystals measured (*7, 8*). Due to the integral nature of these PGSE measurements, the spin motion is averaged over the whole crystal. The implementation of phase encoded imaging enabled the combination of imaging and PGSE to obtain *local* mobility maps. Two-dimensional mobility weighted maps of these crystals have been presented recently, demonstrating the inhomogeneities of the spin mobility throughout the crystal (*12*).

The PGSE signal attenuation is due to spin motion during the time Δ between the two gradient pulses. In the presence of restricted diffusion one can define "the long time limit" for Δ as the time necessary for the confined spins to bounce back and forth between the barriers. At this limit, signal attenuation as a function of the pulsed gradient intensity reveals the Fourier spectrum of the spin density between the barriers, an effect which has been termed diffusive diffraction (*1, 9*). The appearance of this effect is dependent on the uniformity of the interbarrier spacing. In this work we will present such an effect in the $(FA)_2PF_6$ crystals. The typical diffusion coefficient measured for these crystals is $D \sim 2 \times 10^{-4}$ m^2/s (*7, 8*). The spacing between the pulses Δ is limited to 10–15 μs due to spin relaxation. To reach the long time limit it is therefore necessary to measure restricted regions with an interbarrier spacing of the order of 100 μm. This was obtained by artificially damaging the crystal at different locations thus creating separate, and well defined, sections. To probe the results of this crystal sectioning it was essential to locally map the response of the signal as a function of the PGSE gradient intensity. This is the first example of such a mapping in ESR imaging, although it has been demonstrated in nuclear magnetic resonance imaging (see, for example, (*13*)).

2. THEORY

We will now summarize briefly the theory of PGSE of one-dimensionally restricted spins and describe the imaging method we are using to probe local spin dynamics.

1090-7807/02 $35.00

2.1. PGSE of Restricted Diffusion

The standard PGSE sequence is based on a pair of gradient pulses separated by a time period Δ such that in the absence of spin motion during Δ, the dephasing of the magnetization caused by the first pulse is refocused by the second. In the case of spin motion we define $P_s(\mathbf{r} \mid \mathbf{r}', \Delta)$ as the conditional probability that a spin starting at position $\mathbf{r}$ will move to $\mathbf{r}'$ during the time Δ. In the case of sharp pulses where the spin motion during the duration of the pulse can be neglected, the normalized PGSE echo signal is given by

$$E(\mathbf{q}, \Delta) = \int\int d\mathbf{r}\, d\mathbf{r}' \rho(\mathbf{r}) P_s(\mathbf{r} \mid \mathbf{r}', \Delta) \exp(i2\pi \mathbf{q} \cdot (\mathbf{r} - \mathbf{r}')), \quad [1]$$

where $\mathbf{q} = (2\pi)^{-1}\gamma_e \int_0^\delta \mathbf{G}\, dt$. ($\mathbf{G}(t)$ is the gradient pulse and δ its duration.) In the case of diffusive motion the differential equation governing $P_s(\mathbf{r} \mid \mathbf{r}', \Delta)$ is Fick's law,

$$D\nabla^2 P_s = \partial P_s / \partial t, \quad [2]$$

where D is the diffusion coefficient. For one-dimensional motion restricted by rectangular barriers, P_s can be obtained analytically by solving Fick's equation with the suitable boundary conditions. The echo attenuation has been shown by Stejskal and Tanner to be (*17*)

$$E(q, \Delta) = 2\frac{[1 - \cos(2\pi q l)]}{(2\pi q l)^2} + 4(2\pi q l)^2 \times \sum_{n=1}^{\infty} \exp\left(-\frac{n^2\pi^2 D\Delta}{l^2}\right) \frac{1 - (-1)^n \cos(2\pi q l)}{[(2\pi q l)^2 - (n\pi)^2]^2}, \quad [3]$$

where l is the interbarrier spacing. For $\Delta \gg l^2/D$ (the so-called long time limit) the spins "lose memory" of their starting point and $P_s(\mathbf{r} \mid \mathbf{r}', \Delta)$ can be approximated by $\rho(\mathbf{r}')$. We can then write

$$E(q, \infty) = \int\int \rho(\mathbf{r})\rho(\mathbf{r}') \exp[i2\pi \mathbf{q} \cdot (\mathbf{r}' - \mathbf{r})]\, d\mathbf{r}'\, d\mathbf{r} = \left| \int \rho(\mathbf{r}) \exp(i2\pi \mathbf{q} \cdot \mathbf{r})\, d\mathbf{r} \right|^2. \quad [4]$$

For a one-dimensional region of length l the result is

$$E(\mathbf{q}, \infty) = |\sin c(\pi q l)|^2 \quad [5]$$

which is identical to the optical diffraction pattern of a single slit of width l. This effect has therefore been termed diffusive diffraction (*1, 9*). The diffraction minima of $E(\mathbf{q}, \infty)$ should appear at q-values fulfilling the condition $q \cdot l = n$ for integer n-values. It can actually be shown from the analytic solution that the "long time" limit can be relaxed, and this diffraction effect will appear even if $\Delta = l^2/D$ (*1*). As mentioned previously this result neglects the effect of spin motion during the application of the gradient pulses. In recent works the effect of the finite pulse width (δ) has been taken into account as well using a specially developed simulation method (*15, 16*). The result of these simulations was that for a given inter-barrier spacing the diffraction minima will shift to higher values of q such that $q \cdot l = n(1 + \epsilon)$. The value of ϵ has been shown to be dependent on the ratio δ/Δ.

2.2. Combined k-Space q-Space Imaging

In standard magnetic resonance imaging experiments the spatial encoding of the spins is obtained by the application of magnetic field gradients. These gradients, applied either during spin preparation in the form of phase encoding pulses or as static gradients during signal acquisition, construct what has been termed k-space. The local spin density (ignoring relaxation effects) is then given by

$$\rho(x, y, z) = \int\int\int S(k_x, k_y, k_z) \times \exp(2\pi i(k_x x + k_y y + k_z z))\, dx\, dy\, dz, \quad [6]$$

where k_x,k_y, and k_z are a function of the applied gradients (*14*).

Application of the pulsed field gradients in the PGSE sequence results in signal attenuation due to spin motion during the period between the pulses as specified by Eq. [1]. If we now define $\overline{P_s(\mathbf{R}, \Delta)} = \int P_s(r \mid r + R, \Delta)\rho(r)\, dr$ we can write

$$E(\mathbf{q}) = \int \overline{P_s}(\mathbf{R}, \Delta) \exp(i2\pi \mathbf{q} \cdot \mathbf{R})\, d\mathbf{R}, \quad [7]$$

$\overline{P_s}$ being the average probability for any particle to have a displacement of R during the time period Δ between the pulses (*10*). Repeating the sequence with different PGSE gradient intensities constructs what has been termed q-space. The evolution of the PGSE signal in q-space contains information about the average spin dynamics in the sample through the Fourier transform relation existing between $E(\mathbf{q})$ and $\overline{P_s}$. To probe the local dynamics it is necessary to combine diffusion encoding gradients with spatial encoding gradients, and the resulting signal is then described by

$$S(\mathbf{k}, \mathbf{q}) = \int \rho(\mathbf{r}) \exp[i2\pi \mathbf{k} \cdot \mathbf{r}] \int P_s(\mathbf{r} \mid \mathbf{r}', \Delta) \times \exp[i2\pi \mathbf{q} \cdot (\mathbf{r}' - \mathbf{r})]\, d\mathbf{r}\, d\mathbf{r}'. \quad [8]$$

We can now define the local-dynamics contrast as

$$E_\Delta(\mathbf{q}, \mathbf{r}) = \int P_s(\mathbf{r} \mid \mathbf{r}', \Delta) \exp[i2\pi \mathbf{q} \cdot (\mathbf{r}' - \mathbf{r})]\, d\mathbf{r}' \quad [9]$$

and we can write

$$\rho(\mathbf{r})E_{\Delta}(\mathbf{q},\mathbf{r}) = \int S(\mathbf{k},\mathbf{q})\exp[-i2\pi\mathbf{k}\cdot\mathbf{r}]\,d\mathbf{k}. \qquad [10]$$

The effect of the PGSE gradients and the spatial encoding gradients is therefore separable and one can obtain a mapping of the local dynamics (*1*).

3. EXPERIMENT

The measurements were performed on the quasi-one-dimensional organic conductor $(FA)_2PF_6$ in the fringe field of a 7.0-T superconducting magnet at a field of approximately 105 G. A Tecmag LIBRA spectrometer was used, operating at ~300 MHZ. The gradient assembly manufactured at Massey University, New Zealand, included three orthogonal gradient coils each producing 0.2 Tm^{-1} A^{-1}. The relatively long relaxation times of this crystal ($T_1 \sim T_2 \sim 10$ μs) enabled pulsed signal detection at 2τ of up to a few tens of microseconds after excitation. The crystal used for this work was irradiated by a beam of 2 MeV of Helium ions which passed through a slitted mask prior to hitting the crystal. The mask was a commercial electron microscopy grid manufactured by Plano, Germany. The grid included slots of 55 and 125-μm width with an accuracy of ± 5 μm. The effect of the irradiation on the electron spin density was studied using a three-dimensional imaging sequence composed of two phase encoding gradients and a read encoding gradient. The imaging resolution was $(30\mu)^3$. The phase encoding was implemented with half sine pulses created with the clipped L-C resonance circuit (*11*). A detailed description of the imaging implementation can be found elsewhere (*6*). Spin motion was studied using a sequence combining two-dimensional imaging and PGSE. To improve S/N, one of the nonconducting dimensions was not encoded, and therefore the crystal was projected onto the two encoded dimensions. The imaging resolution was therefore (30 μm) $\times$ (30 μm) $\times$ (500 μm), the crystal width being approximately 500 μm. A typical sequence combining 2D imaging and PGSE is presented in Fig. 1. The sequence includes a static read gradient along the y-axis (Fig. 1d), and a phase encoding gradient on the x-axis (Fig. 1c). The x-axis, which is identified as the conducting direction, is also the direction in which the diffusion encoding pulses are applied (Fig. 1b). Due to the short times available for the sequence, the first PGSE pulse and the phase encoding gradient were applied simultaneously. The q-space mapping was obtained by repeating this sequence with different diffusion encoding gradient intensities.

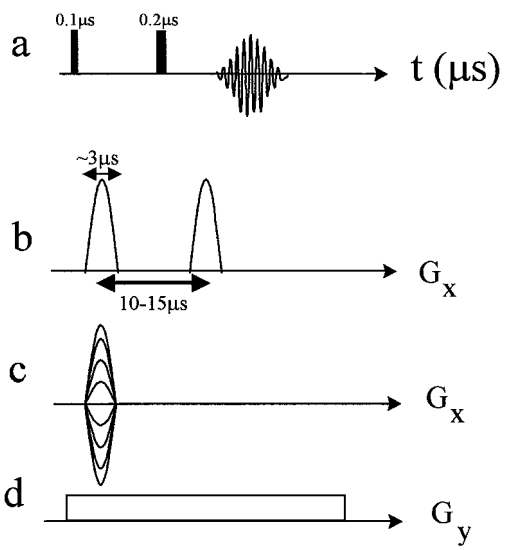

FIG. 1. A typical pulse sequence including a combination of a PGSE pair with a phase encoding gradient on the x axis (b, c), and a read gradient on the y axis (d).

4. RESULTS

The results of crystal irradiation are presented in Fig. 2. Figure 2a is a schematic approximation of the mask position relative to the crystal. The images were reconstructed from a density-weighted three-dimensional pulsed ESR imaging sequence as described previously. The images show 3D isodensity surfaces of the crystal defined by 2 different thresholds. Figure 2c has a higher threshold showing only higher intensity voxels. The conclusion from these images is that there was considerable damage to the crystal's surface in unmasked areas as can be seen in Fig. 2b, but there was also a weaker whole volume damage possibly dividing the crystal into separate sections as is evident in Fig. 2c. Figure 3 presents the q-space evolution of the signal for different regions of the crystal. Figure 3a is the projected two-dimensional image of the crystal. The division of the crystal into sections is apparent. Figures 3b, 3c, and 3d are the q-space evolution of the signal for several pixels in the different regions. The "diffusion diffraction" effect is apparent in Figs. 3b and 3c with the diffraction minima appearing at the expected positions. ROI B is from a section 2-pixels long, therefore approximately 60 μm in length, and ROI A is from a section 4-pixels long, therefore approximately 120 μm long. For $l = 120$ μm and $\Delta = 15$ μs we can calculate $\Delta/(l^2/D) = 0.2$ (assuming $D = 2 \times 10^{-4}$ m^2/s), thus we are on the border of the long time limit. This can account for the smearing of the minima in ROI A as shown in Fig. 3b. A slight shift in the minima between the two Δ values presented in Fig. 3b can possibly be identified, although S/N is not good enough to verify it. This could be attributed to the finite pulse width effect described previously. As mentioned, simulations show that the size of the shift is dependent on the ratio δ/Δ where δ is the pulse width (*15, 16*). For the exact size of the shift it is necessary to simulate our experimental conditions, but the direction of the shift is as expected. The data from ROI D in Fig. 3b are from a region outside of the crystal and are an indication of the noise level. The size of the region was chosen so that the number of pixels averaged is similar to the number of pixels chosen from the other regions. The data from

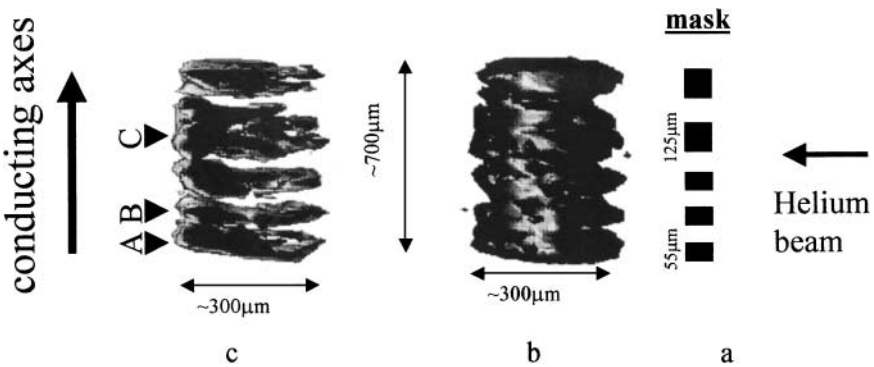

FIG. 2. Isodensity surfaces of an irradiated crystal at 2 different intensity thresholds. (a) The approximate position of the mask relative to the crystal. (b) Threshold ~50% of maximum pixel intensity; (c) Threshold ~25% of maximum.

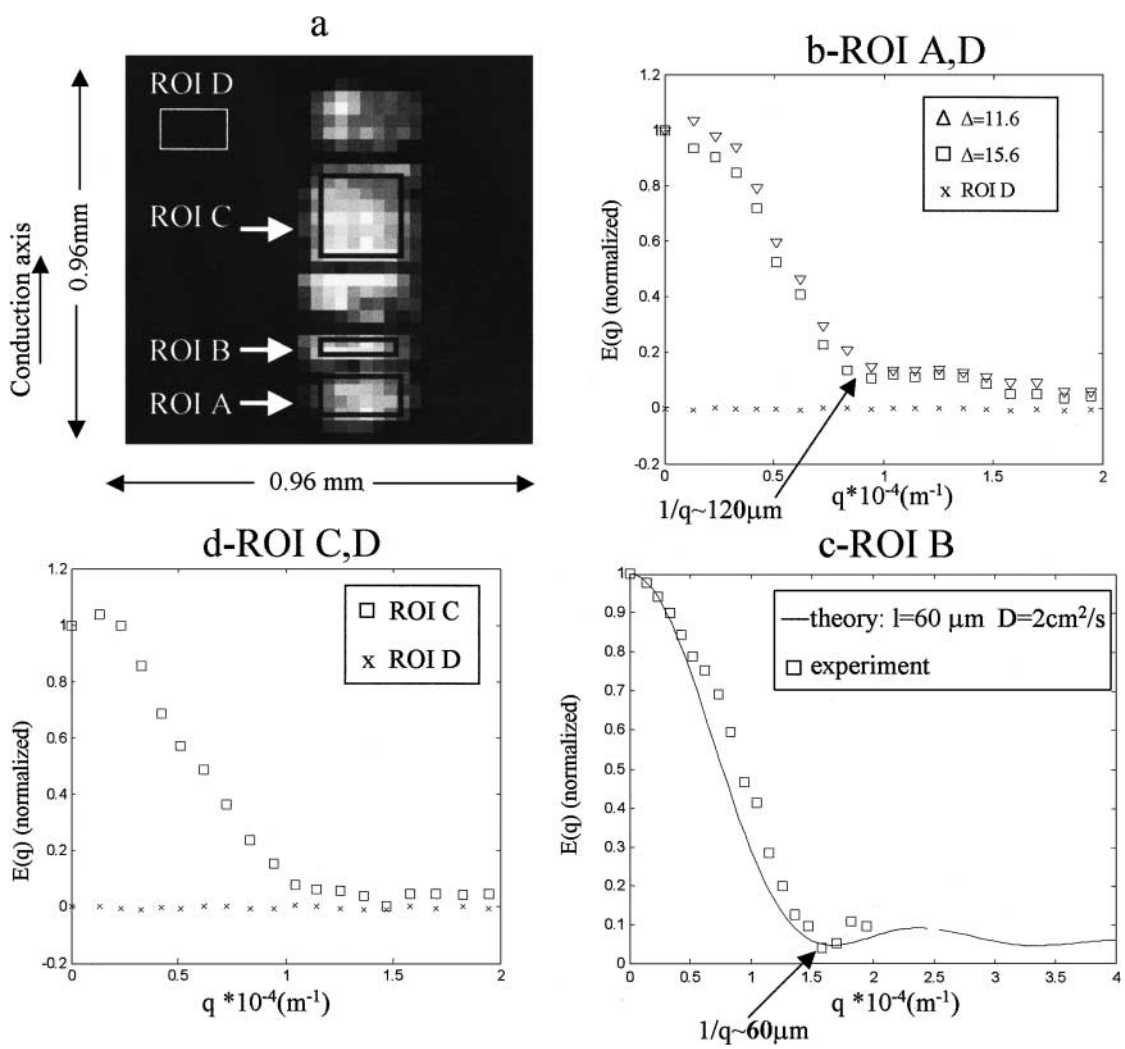

FIG. 3. PGSE attenuation of different regions of the irradiated crystal. The map in (a) was reconstructed from data acquired by a 2D imaging sequence. Pixel size is $(30\ \mu\mathrm{m})^2$.

ROI D were normalized to the value of E(0) in ROI A. In Fig. 3c we show the results of the analytic solution (Eq. [3]) for the diffusion coefficient (D) and interbarrier spacing (l) we expect for ROI B. Although the general diffraction pattern is verified by the fit,it is apparent that significant deviations still exist between this model and the experimental results. This could be attributed to the nonuniformity of the irradiation damage as can be seen in Fig. 2c, leading to a distribution of chain lengths in the probed region. Figure 3d shows the results from ROI C which show a set of pixels where the "diffusion diffraction" effect does not appear. This is attributed to the length of this region which removes us from the long time limit. It should be noted that this region is very nonuniform, as is evident from Fig. 2c, and is partially damaged. This damage is not apparent in the two-dimensional image probably due to the angle of the projection. The data presented are from a small number of pixels in this region which seem to belong to a group of relatively long chains. These were chosen specifically to show the absence of the "diffusion diffraction" effect at what seems to be the breakdown of the long time limit.

5. SUMMARY AND CONCLUDING REMARKS

Combined k-space q-space ESR imaging performed on $(FA)_2PF6$ crystals has been shown to be a tool capable of revealing local dynamic properties of conducting electrons. A qualitative agreement was demonstrated between the experiment and the analytic model of restricted one-dimensional diffusion, but numerical agreement is still lacking. Improvement of the irradiation technique and creating sharper bounderies could possibly give better results. The basic assumption of this work is that the spins of the charge carriers in these quasi-one-dimensional conductors can be treated as a classical particle in a restricted region bouncing back and forth between the boundaries. It would be of interest to miniaturize the interbarrier spacing, causing quantum effects to appear.

ACKNOWLEDGMENTS

This research is supported by the Israel Science Foundation (Grant 28/01). We are grateful to G. Linker and R. Fromknecht of IFP/FZK for the crystal irradiation, and to C. Buschaus, B. Pongs, and T. Wokrina of Karlsruhe University for help in preparation and verification of the irradiation. One of the authors (A.F.) acknowledges financial support by the Horowitz Foundation.

REFERENCES

1. P. T. Callaghan, "Principles of Nuclear Magnetic Resonance Microscopy," Oxford Univ. Press, Oxford/New York (1991).
2. E. Dormann, *Phys. B.* **39,** 221(1983).
3. S. S. Eaton and G. R. Eaton, *in* "EPR" (M. J. Davies, B. C. Gilbert, and K. A. Mclauchlan, Eds.), Vol. 17, p. 109 (2000).
4. N. Devasahayam, S. Subramanian, R. Murugesan, J. A. Cook, M. Afeworki, R. G. Tschudin, J. B. Mitchell, and M. C Krishna, *J. Magn. Reson.* **142,** 168 (2000).
5. G. Placidi, J. A. Brivati, M. Alecci, and A. Sotgiu, *Phys. Med. Biol.* **43,** 1845 (1998).
6. A. Feintuch, G. Alexandrowicz, T. Tashma, Y. Boasson, A. Grayevsky, and N. Kaplan, *J. Magn. Reson.* **142,** 382 (2000).
7. N. Kaplan, E. Dormann, R. Ruf, A. Coy, and P. T. Callaghan, *Phys. Rev. B* **52,** 16385 (1995).
8. T. Tashma, G. Alexandrowicz, N. Kaplan, E. Dormann, A. Grayevsky, and A. Gabay, *Synth. Met.* **106,** 151 (1999).
9. D. G. Cory and A. N. Garroway, *Magn. Reson. Med.* **14,** 485 (1990).
10. J. Karger and W. Heink, *J. Magn. Reson.* **51,** 1 (1983).
11. M. Conradi, A. N. Garroway, D. G. Cory, and J. Miller, *J. Magn. Reson.* **94,** 370 (1991).
12. G. Alexandrowicz, T. Tashma, A. Feintuch, A. Grayevsky, E. Dormann, and N. Kaplan, *Phys. Rev. Lett.* **84,** 2973 (2000).
13. P. T. Callaghan, W. Köckenberger, and J. M. Pope, *J. Magn. Reson. B* **104,** 183 (1994).
14. A. Kumar, D. Welti, and R. R. Ernst, *J. Magn. Reson.* **18,** 69 (1975).
15. A. Duh, A. Mohorič, and J. Stepišnik, *J. Magn. Reson.* **148,** 257 (2000).
16. P. T. Callaghan, *J. Magn. Reson.* **129,** 74 (1997).
17. J. E. Tanner and E. O. Stejskal, *J. Chem. Phys.* **49,** 1768 (1968).